MATERIALS RESEARCH LETTERS

Mater. Res. Lett., 2013
Vol. 1, No. 3, 126–132, http://dx.doi.org/10.1080/21663831.2013.792019

Taylor & Francis
Taylor & Francis Group

www.tandfonline.com/toc/tmrl21/current

Pure-Shuffle Nucleation of Deformation Twins in Hexagonal-Close-Packed Metals

J. Wang[a]*, S.K. Yadav[a], J.P. Hirth[b], C.N. Tomé[a] and I.J. Beyerlein[c]

[a]*MST-8, Los Alamos National Laboratory, Los Alamos, NM 87545, USA;* [b]*MPA-CINT, Los Alamos National Laboratory, Los Alamos, NM 87545 USA;* [c]*T-3, Los Alamos National Laboratory, Los Alamos, NM 87545 USA*

(*Received 28 March 2013; final form 28 March 2013*)

Supplementary Material Available Online

The propagation of deformation twins in hexagonal-close-packed metals is commonly described by a conventional glide-shuffle mechanism. The widely accepted convention is that this process is also responsible for twin nucleation, but lacks direct confirmation. Using atomistic simulations, we identify an unconventional pure-shuffle mechanism for the nucleation of $(\bar{1}012)$ twins, which then grow through the conventional glide-shuffle mechanism entailing the glide of twinning disconnections. The pure-shuffle nucleation of twins at grain boundaries can be ascribed to a high-stress concentration and pre-existing grain boundary dislocations.

Keywords: Twin Nucleation, Pure-Shuffle, Grain Boundary, Magnesium, Atomistic Simulations

The atomic motions in the formation of a twin are classified as pure glide, glide-(plus) shuffle, and pure-shuffle, as summarized in Figure 23-5 in [1]. The pure-shuffle can be associated with parallel or general-shuffle vectors. Models for the propagation of twins entail the motion of twinning dislocations or disconnections (TDs). [1,2] The latter is more descriptive since some of the defects have no net dislocation character. In face-centered-cubic (FCC) and body-centered-cubic (BCC) metals, the TDs are usually of the pure glide type, as verified in atomistic simulations [3–5] and in high-resolution transmission electron microscopy observations. [6,7] However, there are cases where the TDs have zonal character with pure-shuffle or glide-shuffle of the parallel type. These include FCC metals, [8–12] BCC metals, [13] and hexagonal-close-packed (HCP) metals. [14] In some of the cases, the zonal TDs are formed as a consequence of the formation of emissary dislocations. [12,13] In HCP, the TDs associated with $K_1 = \{\bar{1}012\}$ twins have step heights of two planes and are always of the glide-shuffle type. [15–17] The formation mechanism is less clear for twin nucleation, particularly in HCP metals, which are the most likely to form deformation twins when strained because of an insufficient number of slip systems. [2] However, twin nucleation in HCP metals is less understood in terms of both kinetics and energetics.

The focus of the present work is on twin nucleation. Models for twin nucleation include the pole mechanism, [18] where the critical event is the non-planar bowout-dissociation of a c dislocation, forming a single partial that subsequently winds around a 'pole' dislocation to create a $[10\bar{1}1](\bar{1}012)$ twin. There are also constraints when the TD rotates by an integer times 2π. [1,19] Other models envision the heterogeneous nucleation and emission of TDs at boundaries [20]; near cracks [21]; as a consequence of the interaction of coplanar/non-coplanar dislocation dipoles at high velocity [3,4]; or from more complex non-planar dissociation reactions. [22] In these models, except for the pole model, the nucleation event is either ignored or involves arrays of like-sign TDs with accompanying stress fields. For the case of emission of a nucleus from a grain boundary (GB), atomic-scale studies, using density-function-theory (DFT) and molecular dynamics (MD) with empirical interatomic potentials, showed that neither a single TD nor an array of like-sign TDs lead to the formation of a stable nucleus. [15] Instead, the stable twin nucleus must contain multiple unit TDs and an opposite sign TD of larger Burgers vector in a zonal arrangement. The growth of the nucleus, however, still took place by glide-shuffle. [16] Shuffle mechanisms, with no distinction between pure-shuffle and glide-shuffle, have been suggested for

*Corresponding author. Email: wangj6@lanl.gov

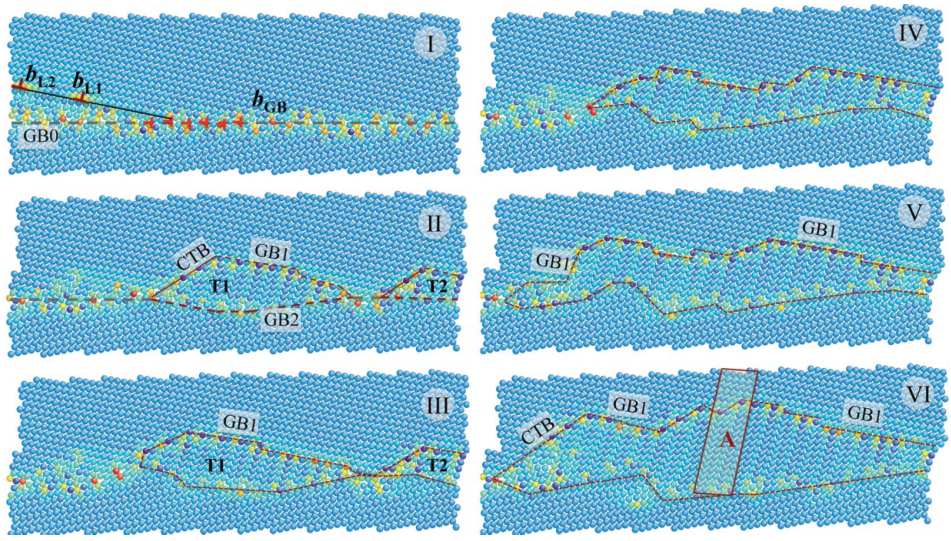

Figure 1. Changes in atomic structures of GB: (I) initial 10.6° tilt boundary; tilt axis [11$\bar{2}$0] is pointed out of the paper. (II) to (VI): nucleation and growth of twin embryos at GBs. Atoms are colored according to their excess energy. Three types of boundaries outline the twin embryo, CTB, GB1 that bounds the basal plane in the matrix and the prismatic plane in the twin, and GB2 that is associated with the dissociation of the original GB. T1 and T2 indicate two embryos in twin orientation with respect to the top grain. The region marked as A in (VI) is shown in detail in Figure 2.

phase transformations. [23,24] No direct confirmation of a shuffle nucleation event for phase transformations or for deformation twinning has been obtained by either high-resolution transmission electron microscopy or by atomistic simulation.

In this work, we revisit the previous MD simulations of heterogeneous nucleation of $K_1 = (\bar{1}012)$ twins at symmetric tilt grain boundaries. [25,26] We concentrate on the analysis of atomic shuffles, and show that the nucleus forms by a pure-shuffle mechanism.

Taking Mg as a prototype material, an embedded atom method potential for Mg [27] is employed in the MD simulations. MD simulations include two stages. The details are addressed in Figure S1 in the Supplementary Material. Stage I is to construct and relax a bicrystal model [26,28] and Stage II is to construct a dislocation-boundary interaction model. [29,30] We simulated the interaction of the symmetrical tilt grain boundaries with approaching lattice dislocations. Starting with the relaxed bicrystal model, [26] we introduce four mixed basal lattice dislocations, $< a >\{0001\}$, into the bicrystal, forming a coplanar dislocation pile-up, by the application of the anisotropic Barnett–Lothe solutions for the displacement field of a dislocation in a bicrystal. [31] The dislocation line is parallel to the tilt axis. Their initial positions are estimated from the coplanar stressed single-ended pile-up model. [1] MD simulations were carried out at a constant temperature of 50 K, and the resolved shear stress on the glide plane is dynamically controlled at the constant level of 100 MPa.

The nucleation, coalescence, and growth of $(\bar{1}012)$ twin nuclei were observed at the tilt walls with a tilt angle of 10.6° and 17.3°, respectively. [25,26] Figure S2 and Movie01 in the Supplementary Material show the detailed processes at the wall with a tilt angle of 10.6°. Similar processes also occurred for the other tilt wall. Figure 1 shows six snapshots of atomic structures during the nucleation and growth of twins at the tilt boundary. Figure 1(I) is the initial GB structure at zero applied stress. When the first two lattice dislocations enter the GB, Figure 1(II) shows the formation of two twin embryos, T1 and T2. The tilt wall between T1 and T2 remains unchanged. The twins are surrounded by $(\bar{1}012)$ coherent twin boundaries (CTBs) and two GBs (GB1 and GB2). GB1 is defined by a basal plane in the top grain being parallel to a prismatic plane in the nucleus (the B/P boundary, following [12]). When the third lattice dislocation enters the GB, Figure 1(III) and 1(IV) shows that the twin embryos coalesce and grow quickly. The coalescence takes place by the nucleation of a new twin embryo in the region between T1 and T2. The fourth lattice dislocation is stopped at the CTB (Figure 1(V)) and reacts with the GBDs, resulting in the growth of the twin embryo toward the left (Figure 1(VI)). In addition, CTB steps form in the GB1 and move along it during the growth of the twin embryos.

To provide an insight into the nucleation event, we tracked the change in position of atoms in the region A indicated in Figure 1(VI). Figure 2(I) shows the initial atomic structure and Figure 2(II) shows a twin structure at the bottom, outlined by the red dashed line. Observe the atoms belong to a prismatic plane-shuffle to a basal configuration. The transition from 2(I) to 2(II) is referred to as *twin nucleation*. The change from 2(II) to 2(III), where the top grain shifts by one atomic plane relative to the twin along the GB1 while the twin nucleus does not

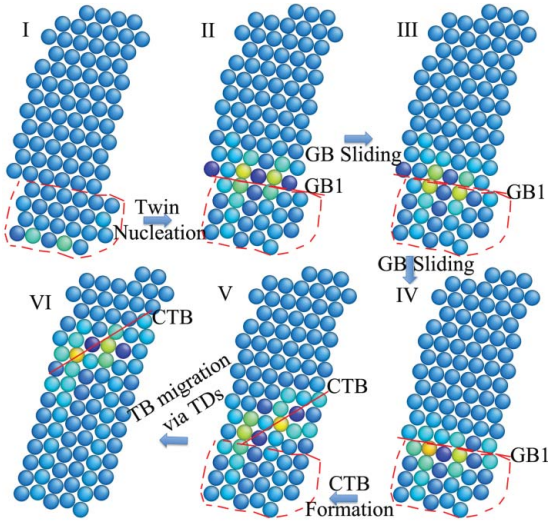

Figure 2. Changes in atomic structures of the region A marked in Figure 1(VI), showing the processes of the nucleation and growth of twins corresponding to the six snapshots in Figure 1. (I) Initial structure; (II) nucleation of twin: observe transformation of prism into basal planes via shuffle; (II) to (III) to (IV): the top grain shifts relative to the twin via the sliding of GB1; (V) CTBs formation; and (VI) growth of the twin via gliding of twinning dislocations. All atoms are colored according to their excess energy.

grow, is referred to as *GB sliding*. Accompanying the sliding of the top grain toward the right, the region between T1 and T2 was sheared (not shown in Figure 2) and, as a consequence, the twin embryos T1 and T2 coalesce and a new twin embryo forms in the region between T1 and T2 (Figure 1(IV)). The change from 2(IV) to 2(V), where the twin embryo grows upwards by four atomic layers and the CTB forms, is referred to as *CTB formation*. Thereafter, the twin grows normal to the CTB in 2(VI), which is referred to as *CTB migration*. In the following, we address the four processes, *twin nucleation*, *GB sliding*, *CTB formation* and *CTB migration*.

The relative displacements of atoms in Figure 2(II) with respect to Figure 2(I) are plotted in Figure 3(a). The matrix is displaced toward the GB because of the contraction in the y direction accompanying twin formation. The displacements in the twin demonstrate that *twin nucleation* is accomplished by a pure-shuffle mechanism. The coherent twin nucleus in Figure 2(II) is nominally rotated by 90° (see below) about the $[11\bar{2}0]$ z-axis so that the $(1\bar{1}00)$ prismatic plane in the nucleus becomes parallel to the basal plane in the matrix, (B/P) and vice versa. The twin boundaries are all rotated relative to the K_1 plane. The displacements in a natural dichromatic complex, [32,33] shown in Figure 3(b), agree with the MD results in Figure 3(a). In addition, there are two transformation strains, $\varepsilon_{xx} = 2\frac{\kappa-\sqrt{3}}{\kappa+\sqrt{3}}$ and $\varepsilon_{yy} = -\varepsilon_{xx}$ (-0.065 and 0.065 for Mg, respectively). The ε_{yy} strain accounts for the displacements in the matrix in Figure 3(a). The relaxations to Figure 3(b) require accommodation strain and rotation associated with added misfit defects in the GBs. For the nucleation process, the interfaces are coherent. Figure 3(c) is a coherent dichromatic complex (CDC, [32,33]). The CDC reveals the displacements in nucleus formation which correspond to those of a pure-shuffle mechanism. The corners of a unit cell in the CDC remain fixed and therefore there are no displacements of the matrix. The red vectors are the shuffle vectors.

Twin nucleation via the pure-shuffle mechanism is thus tantamount to a rotation of the nucleus into twin orientation. As shown in Figure 23-3 in [1], a CTB of large extent can be envisioned as a tilt wall of intrinsic dislocations. The rotation of 86.22° associated with the tilt wall is equally partitioned between the twin and matrix for a twin boundary to a large extent. However, in the case of a small nucleus, the stiffness of the surrounding matrix prevents this partitioning and all rotation (3.78°) is imposed on the nucleus and is accommodated at the nucleus interface. The boundary of the rotated nucleus can be regarded as a disclination quadrupole with the disclination fields canceling to first order. [34] Hence, at the early stages of nucleation and growth, the rotation is not partitioned, and the interface is (0001) in the matrix parallel to $(1\bar{1}00)$ in the twin. That is, it is the true twin interface with the partitioning removed. The true twin boundary of large extent would be (0001) plus 1.9° in the matrix or $(1\bar{1}00)$ minus 1.9° in the twin, since the partitioned 1.9° is removed to the twin. [35,36] If this removal of partitioning were not to occur in the large twin boundary, then large local elastic strains would be needed to make the interfaces the true (incoherent) twin interfaces.

Atomistic simulations demonstrate the change in interface structure when a crystallite is rotated by 90° and embedded in the matrix. In MD simulations, Figure 4(a) shows that the initial interfaces consist of $(0001) \parallel (1\bar{1}00)_T$ and $(1\bar{1}00) \parallel (0001)_T$ (referred to as B/P or P/B) when the nucleus is small. The initial nucleus is embedded in a matrix that is subjected to the strains 0.065 along and -0.065 along [0001]. MD simulations were carried out at 10 K. Atoms are colored according to their excess energy: the lowest in the blue and the highest in the red. Figure 4(b) shows that the interfaces tend to rotate by 1.9° to form CTBs and incoherent twin boundaries (ITBs) as the nucleus grows. Correspondingly, the CTBs marked in Figure 4(b) may not be perfect accompanying the growth of the embedded crystal. Particularly, visible dislocations could form along the CTBs or at the corners between CTBs and B/Ps or P/Bs. The details can be observed in Movie02 in the Supplementary Material and show the interfaces for a crystallite with a 90° rotation embedded in the matrix and the corresponding change toward the equilibrium CTB and ITB (in CTB) interfaces as the twin grows.

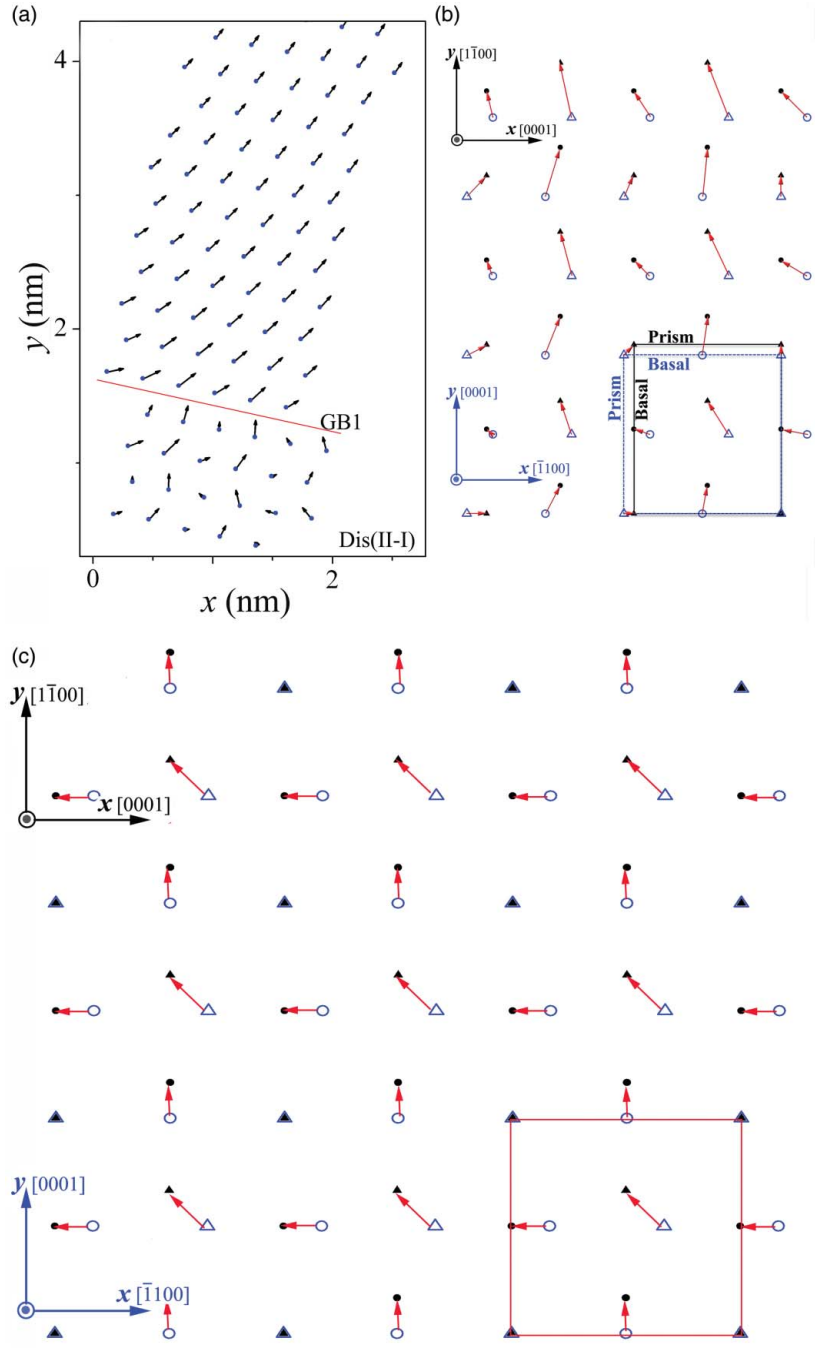

Figure 3. Twin nucleation via a pure-shuffle mechanism. (a) Relative displacements of atoms in the twin structure of Figure 2(II) with respect to the initial structure of Figure 2(I), revealing that twin nucleation corresponds to a rotation of the initial crystal by nominally 90° via a pure-shuffle mechanism. (b) Nature dichromatic complex corresponding to the crystal rotation in (a). The red arrows show the relative displacements corresponding to the rotation. The difference in the side length of the two rectangles indicates the associated transformation strains with respect to the *x*- and *y*- directions. (c) CDC corresponding to the crystal rotation in (a). A unit cell is outlined by the red rectangle. The red arrows show the shuffle vectors. The open blue symbols represent the initial crystal and the solid black symbols represent the final crystal.

We further examined the possibility of homogeneous nucleation via a pure-shuffle mechanism by a DFT calculation. The DFT simulations employed the Vienna *ab initio* simulation package, with the Perdew–Burke–Ernzerhof generalized gradient approximation functional and projector-augmented wave frozen-core potentials. [37] An energy cut-off of 265 eV for the plane wave expansion of the wave functions was used. The calculated and experimental values of lattice parameters, bulk modulus, and elastic constants of Mg compare well, indicating the robustness of the computational settings chosen. We start with a cuboid-shaped supercell (four atoms).

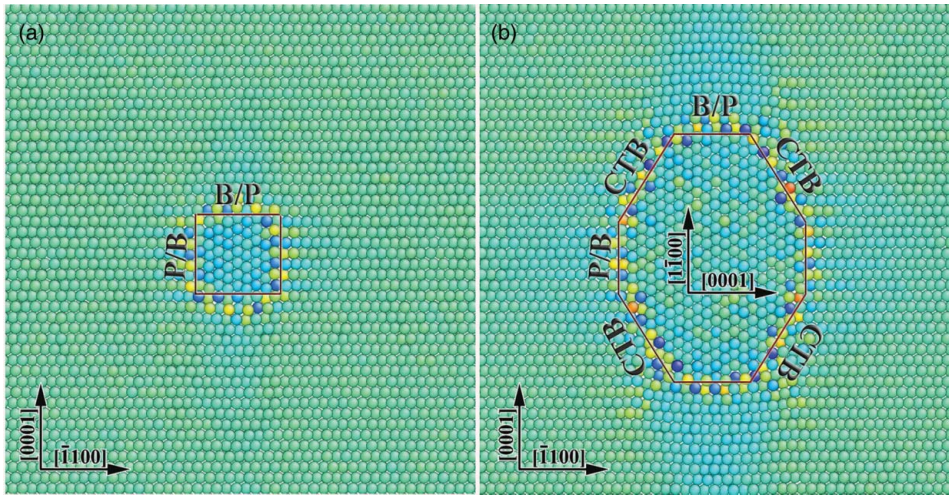

Figure 4. Atomic structure of a twin nucleus in a single crystal. (a) The initial nucleus is embedded in a matrix and the initial interfaces consist of $(0001)\,\|(1\bar{1}00)_T$ and $(1\bar{1}00)\|(0001)_T$ (referred to as B/P or P/B) when the nucleus is small. (b) The interfaces tend to rotate by 1.9° to form CTBs and incoherent ITBs as the nucleus grows. Atoms are colored according to their excess energy: the lowest in the blue and the highest in the red.

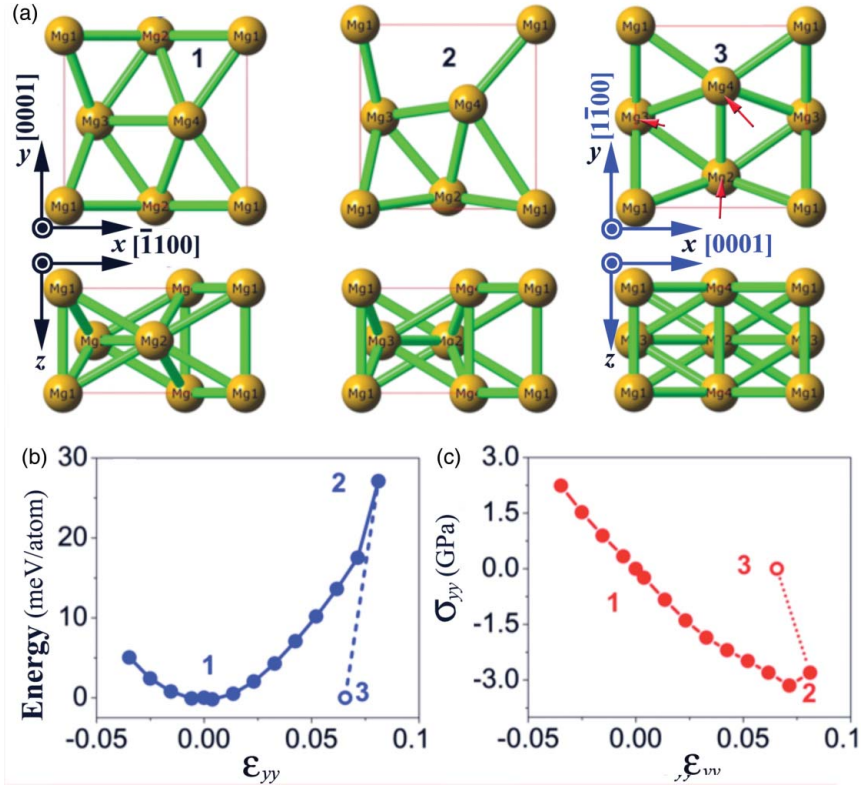

Figure 5. DFT calculations examine the crystal rotation via a pure-shuffle mechanism. (a) Three sets of atomic structures corresponding to the engineering strains, 0.0, 0.075, and 0.065 with respect to the initial orientation. The crystal rotates nominally 90° about the $[11\bar{2}0]$ z-axis. (b) Change in the excess energy of atoms with the applied strain. (c) Change in the tensile stress with the applied strain. Red arrows indicate the collective shuffle vectors.

To achieve a high level of accuracy, a Monkhorst–Pack k-point mesh of $13 \times 13 \times 13$ was used in the simulation. During the calculation, the Hellmann–Feynman force on each atom in the computational supercell was made to converge to 0.01 eV/Å or less. Corresponding to the extension twin, a uniform extension strain was applied along the [0001] direction while allowing stress relaxation in the other two directions. During the relaxation, symmetry constraints were not applied to reduce the artificial force.

Figure 5(a) shows that the crystal rotates nominally 90° about the $[11\bar{2}0]$ direction via a pure-shuffle

mechanism. The displacements are indicated by the red arrows in Figure 5(a). The critical strain leading to the rotation is 7.5% (comparable to the transformation strain 6.5%) and a uniaxial tensile stress of 3.0 GPa. While this process does not correspond to nucleation within a perfect crystal, it does show that large strains and a huge thermodynamic driving force would be needed in such a nucleation process. While this result essentially rules out a homogeneous nucleation process, it also suggests that the large incompatibility stresses at GBs would enhance the likelihod of heterogeneous nucleation. Another pertinent factor in nucleation at a GB would be the relative changes in net GB energy. Figure 6 shows the magnified atomic structures before and after twin nucleation at the tilt wall. Accompanying the nucleation, three new boundaries form, $(\bar{1}012)$ CTBs and two GBs (GB1 and GB2). The GB1 bounds the basal plane in the matrix and the prismatic plane in the twin (referred to as B/P in Figure 4). The GB2 is associated with the dissociation of the original symmetric tilt grain boundary (STGB). The GBs excess energies are of 122, 170, 230, and 340 mJ/m^2, corresponding to CTB, GB1, GB2, and the STGB, respectively, [26, 38] so the surface energy change is small when the twin forms.

GB sliding is clearly identified by tracking the displacement of the top grain with respect to the twin. Going from Figure 2(II) to 2(III) to 2(IV), the top grain moves toward the right along the GB1, as shown in Figure 7(a) in the Supplementary Material. As a consequence, the region between the twin embryos T1 and T2 is sheared, facilitating the nucleation of new twin embryos and the coalescence of T1 and T2. Through the same mechanism, multiple twin embryos nucleate and coalesce, as observed in Figure S2 and Movie01 in the Supplementary Material. *CTB formation* naturally occurs as the twins grow. The CTB acquires the equilibrium-partitioned configuration. This requires the presence of dislocations at the ends of the CTB segments to accommodate the partitioning. The extrinsic dislocations that initiate the entire process supply the needed Burgers vector content. We suggest that this is a catalyzing contribution, in addition to the added stresses, of the extrinsic dislocations to the overall process. Later twin growth normal to the CTB occurs by TD motion by the usual glide-shuffle mechanism. *CTB migration via TDs* is evidenced by the relative displacements in Figure 7(b). The CTB migrates upwards by four atomic planes as a consequence of the glide of two TDs by a glide-shuffle mechanism. Along the red dashed lines, atoms experience a non-uniform shear along the twinning direction and the average shear displacement is equal to the magnitude of Burgers vector of a TD. Accompanying the TD motion, alternate layers shuffle to complete the glide-shuffle process. [12,15,39]

In summary, MD simulations and DFT calculations demonstrate the nucleation of twins in HCP structure via a pure-shuffle mechanism. After nucleation, the twins grow via the conventional glide-shuffle mechanism, i.e. the glide of twinning dislocations along the CTBs. Large transformation strains are associated with the rotation via the pure-shuffle mechanism, implying the need for heterogeneous nucleation at GBs, which is consistent with experimental observations. [25,40]

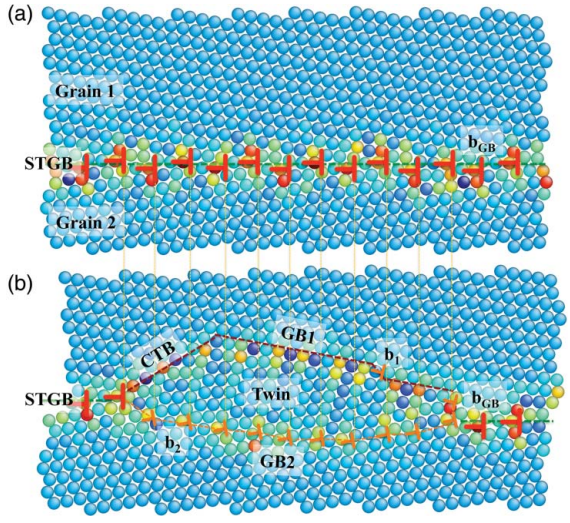

Figure 6. Atomic structures correspond to twin nucleation at STGBs. Before twinning, GB dislocations, $\boldsymbol{b_{GB}}$, are uniformly distributed along the STGB with an average spacing of 0.7 nm (including three atomic planes), and the Burgers vector is equal to (0, 0.256, 0) nm [25]. After twinning, GBDs dissociate into $\boldsymbol{b}_1$ and $\boldsymbol{b}_2$ in the two new boundaries, GB1 and GB2, respectively.

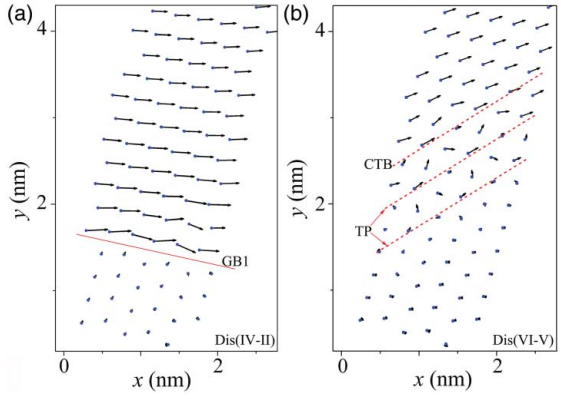

Figure 7. (a) The relative displacements of atoms in Figure 2(IV) with respect to Figure 2(II) reveal the sliding of the top grain with respect to the twin along the GB1. (b) The relative displacements of atoms in Figure 2(VI) with respect to Figure 2(V) reveal the growth of the twin via the shear-shuffle mechanism in association with the glide of twinning dislocations.

Supplementary online material. A more detailed information on experiments is available at http://dx.doi.org/10.1080/21663831.2013.792019.

Acknowledgements The authors acknowledge full support from Office of Basic Energy Sciences, Project FWP 06SCPE401, under U.S. DOE Contract No. W-7405-ENG-36. The authors are grateful for the helpful comments from Prof. Robert Pond.

References

[1] Hirth JP, Lothe J. Theory of dislocations. Melbourne, FL: Krieger; 1992.
[2] Christian JW, Mahajan S. Deformation twinning. Prog Mater Sci. 1995;39(1):1–157.
[3] Wang J, Huang H. Novel deformation mechanism of twinned nanowires. Appl Phys Lett. 2006;88:203112.
[4] Chu HJ, Wang J, Beyerlein IJ. Anomalous reactions of a supersonic coplanar dislocation dipole: bypass or twinning? Scr Mater. 2012;67:69–72.
[5] Wang J, Huang H. Shockley partial dislocations to twin: another formation mechanism and generic driving force. Appl Phys Lett. 2004;85:5983–5985.
[6] Zhu YT, Liao XZ, Wu XL. Deformation twinning in nanocrystalline materials. Prog Mater Sci. 2012;57:1–62.
[7] Li N, Wang J, Huang JY, Misra A, Zhang X. Influence of slip transmission on the migration of incoherent twin boundaries in epitaxial nanotwinned Cu. Scr Mater. 2011;64:149–152.
[8] Wang J, Li N, Anderoglug O, Zhang X, Misra A, Huang JY, Hirth JP. Detwinning mechanisms for growth twins in face-centered cubic metals. Acta Mater. 2010;58: 2262–2270.
[9] Liu L, Wang J, Gong SK, Mao SX. High resolution transmission electron microscope observation of zero-strain deformation twinning mechanisms in Ag. Phys Rev Lett. 2011;106:175504.
[10] Wu XL, Liao XZ, Srinivasan SG, Zhou F, Lavernia EJ, Valiev RZ, Zhu YT. New deformation twinning mechanism generates zero macroscopic strain in nanocrystalline metals. Phys Rev Lett. 2008;100:095701.
[11] Li BQ, Li B, Wang YB, Sui ML, Ma E. Twinning mechanism via synchronized activation of partial dislocations in face-centered-cubic materials. Scr Mater. 2011;64(9):852–855.
[12] Serra A, Bacon DJ, Pond RC. The crystallography and core structure of twinning dislocations in H.C.P. metals. Acta Metall. 1988;36:3183–3203.
[13] Wasilewski RJ. Surface distortions in twinned niobium (Columbium) crystals. Metall Trans. 1970;1:1617–1622.
[14] Dubertret A, Le Lann A. Development of a new model for atom movement in twinning. Phys Status Solidi 1980;60:145–151.
[15] Wang J, Hoagland RG, Hirth JP, Capolungo L, Beyerlein IJ, Tomé CN. Nucleation of a (-1012) twin in hexagonal close-packed crystals. Scr Mater. 2009;61:903–906.
[16] Wang J, Hirth JP, Tomé CN. (-1012) Twinning nucleation mechanisms in hexagonal-close-packed crystals. Acta Mater. 2009;57(18):5521–5530.
[17] Serra A, Bacon DJ. A new model for {10-12} twin growth in hcp metals. Philos Mag A. 1996;73:333–343.
[18] Thompson N, Millard DJ. Twin formation in cadmium. Philos Mag. 1952;43:422–440.
[19] Basinski ZS, Szczerba MS, Embury JD. Dislocation mechanisms for twinning in BCC and FCC crystals. In: Yoo, MH, Wuttig, M, editors. Twinning in advanced materials. Warrendale, PA: TMS; 1994. p. 69–75.
[20] Han WZ, Carpenter JS, Wang J, Beyerlein IJ, Mara NA. Atomic-level study of twin nucleation from face-centered-cubic/body-centered-cubic interfaces in nanolamellar composites. Appl Phys Lett. 2012;100: 011911.
[21] Shan ZW, Lu L, Minor A, Stach EA, Mao SX. The effect of twin plane spacing on the deformation of copper containing a high density of growth twins. JOM 2008;60(9):71–74.
[22] Mendelson S. Zonal dislocations and twin lamellae in h.c.p. metals. Mater Sci Eng. 1969;4(4):231–242.
[23] Olson GB, Cohen M. A general mechanism of martensitic nucleation: part I. General concepts and the FCC → HCP transformation. Metall Trans A. 1976;7:1897–1904.
[24] Aaronson HI, Hall MG. A history of the controversy over the roles of shear and diffusion in plate formation above M_d and a comparison of the atomic mechanism of these processes. Metall Mater Trans A. 1994;25A:1797–1819.
[25] Tomé CN, Beyerlein IJ, Wang J, McCabe RJ. A multiscale statistical study of twinning in magnesium. JOM 2011;63(3):19–23.
[26] Wang J, Beyerlein IJ. Atomic structures of symmetric tilt grain boundaries in hexagonal close packed (hcp) crystals. Modell Simul Mater Sci Eng. 2012;20:024002.
[27] Liu XY, Adams JB, Ercolessi F, Moriarty JA. EAM potential for magnesium from quantum mechanical forces. Modell Simul Mater Sci Eng. 1996;4:293–303.
[28] Wang J, Beyerlein IJ. Atomic structures of [0-110] symmetric tilt grain boundaries in hexagonal close-packed (hcp) crystals. Metall Mater Trans A. 2012;43A:3556–3569.
[29] Wang J, Beyerlein IJ, Hirth JP, Tomé CN. Twinning dislocations on {-1011} and {-1013} planes in hexagonal close-packed crystals. Acta Mater. 2011;59(10): 3990–4001.
[30] Wang J, Beyerlein IJ, Hirth JP. Nucleation of elementary {-1011} and {-1013} twinning dislocations at a twin boundary in hexagonal close-packed crystals. Modell Simul Mater Sci Eng. 2012;20:024001.
[31] Barnett DM, Lothe J. An image force theorem for dislocations in anisotropic bicrystals. J Phys F. 1974;4: 1618–1635.
[32] Pond RC. Line defects in interfaces. In: Nabarro FRN, editor. Dislocations in solids. Vol. 8, Chap. 38, Amsterdam: North-Holland; 1989. p. 1–66.
[33] Hirth JP, Pond RC, Hoagland RG, Liu XY, Wang J, Interface defects, reference spaces and the Frank–Bilby equation. Prog Mater Sci. 2013;58:749–823.
[34] Hirth JP, Pond RC, Lothe J. Disconnections in tilt walls. Acta Mater. 2006;54:4237–4245.
[35] Wang J, Hirth JP, Pond RC, Howe JM. Rotational partitioning at two-phase interfaces. Acta Mater. 2011;59(1):241–251.
[36] Wang J, Li N, Misra A. Structure and stability of Σ3 grain boundaries in face centered cubic metals. Philos Mag. 2013;93:315–327.
[37] Kresse G, Hafner J. *Ab initio* molecular dynamics for liquid metals. Phys Rev B. 1993;47:558–561.
[38] Wang J, Liu L, Tomé CN, Mao SX, Gong SK. Twinning and de-twinning via glide and climb of twinning dislocations along serrated coherent twin boundaries in hexagonal-close-packed metals. Mater Res Lett. 2013. DOI:10.1080/21663831.2013.779601
[39] Li B, Ma E. Zonal dislocations mediating {10-11} <10-1-2> twinning in magnesium. Acta Mater. 2009;57: 1734–1743.
[40] Wang L, Eisenlohr P, Yang Y, Bieler TR, Crimp MA. Nucleation of paired twins at grain boundaries in titanium. Scr Mater. 2010;63:827–830.